Semisynthetic zigzag optical lattice for ultracold bosons

E. Anisimovas, M. Račiūnas, C. Sträter, A. Eckardt, I. B. Spielman, and G. Juzeliūnas

Phys. Rev. A **94**, 063632 — Published 22 December 2016

DOI: 10.1103/PhysRevA.94.063632

Semi-synthetic zigzag optical lattice for ultracold bosons

E. Anisimovas,[1,*] M. Račiūnas,[1] C. Sträter,[2,†] A. Eckardt,[2,‡] I. B. Spielman,[3,4,§] and G. Juzeliūnas[1,¶]

[1] *Institute of Theoretical Physics and Astronomy, Vilnius University, Saulėtekio 3, LT-10222 Vilnius, Lithuania*
[2] *Max-Planck-Institut für Physik komplexer Systeme, Nöthnitzer Straße 38, D-01187 Dresden, Germany*
[3] *Joint Quantum Institute, University of Maryland, College Park, Maryland 20742-4111, USA*
[4] *National Institute of Standards and Technology, Gaithersburg, Maryland 20899, USA*

(Dated: November 28, 2016)

We propose a cold-atom realization of a zigzag ladder. The two legs of the ladder correspond to a "synthetic" dimension given by two internal (spin) states of the atoms, so that tunneling between them can be realized as a laser-assisted process. The zigzag geometry is achieved by employing a spin-dependent optical lattice with the site position depending on the internal atomic state, i. e. on the ladder's leg. The lattice offers a possibility to tune the single-particle dispersion from a double-well to a single-minimum configuration. In contrast to previously considered semi-synthetic lattices with a square geometry, the tunneling in the synthetic dimension is accompanied by spatial displacements of atoms. Therefore, the atom-atom interactions are nonlocal and act along the diagonal (semi-synthetic) direction. We investigate the ground-state properties of the system for the case of strongly interacting bosons. In particular, we find that the interplay between the frustration induced by the magnetic field and the interactions gives rise to an interesting gapped phase at fractional filling factors corresponding to one particle per magnetic unit cell.

PACS numbers: 73.43.-f,67.85.-d,71.10.Hf

I. INTRODUCTION

Optical lattices provide a unique tool for simulating quantum condensed matter physics using ultracold atoms [1–3]. These lattices can be enriched by introducing laser-coupled internal atomic states [4–9] that can play the role of an extra "synthetic" dimension [10–12]. For example, a semi-synthetic square lattice results from the combination of the interlayer tunneling among the sites of a one-dimensional optical lattice and laser-assisted transitions between the onsite atomic levels. If the laser coupling is accompanied by a recoil in the lattice direction, the semi-synthetic lattice acquires a uniform magnetic flux traversing the square plaquettes [11]. This leads to the formation of chiral edge states in the resulting quantum Hall ribbon [11, 13–16]. A characteristic feature of the square geometry is that the atom-atom interaction is long-ranged in the synthetic dimension but short-ranged in the real dimension [11, 17–19].

In this work, we depart from the square geometry and find the ground states of a semi-synthetic optical *zigzag* lattice which can be created combining a spin-dependent one-dimensional optical lattice with laser-induced transitions between the atomic internal states [20]. The lattice is affected by a tunable homogeneous magnetic flux, and furthermore features nonlocal interactions along the semi-synthetic directions that connect different internal states situated at different spatial locations, see also Ref. 21. Generation of magnetic fluxes in an effectively one-dimensional setting is intriguing and was recently considered in Ref. 22. Nonlocal interactions are also an important goal in recent experiments, and such interactions have been engineered via superexchange [23–26] dipole-dipole coupling [27–30], or Rydberg dressing [31–34]. We investigate the ground-state properties of the proposed system for the case of bosonic atoms with strong interactions using the density-matrix renormalization group [35–37] calculations. We find that the interplay between the frustration induced by the magnetic flux and the interactions gives rise to an interesting gapped phase at fractional per-site filling fractions corresponding to one particle per magnetic unit cell.

The paper has the following structure. The single-particle model is formulated in Sec. II A introducing the experimentally motivated lattice setup. The model is solved and analyzed in Sec. II B-II D, in particular, in Sec. II D we explore the manifestation of the resulting band structure via Bloch oscillations of a wave packet in a tilted lattice. Section III is devoted to the many-body phases supported by the semi-synthetic zigzag lattice. The concluding Sec. IV summarizes the findings.

II. SINGLE-PARTICLE HAMILTONIAN

A. Lattice setup

We consider bosonic atoms with two relevant internal states labeled with the (quasi-)spin index $s = \pm 1$. To cre-

* egidijus.anisimovas@ff.vu.lt
† cstraeter@pks.mpg.de
‡ eckardt@pks.mpg.de
§ ian.spielman@nist.gov
¶ gediminas.juzeliunas@tfai.vu.lt

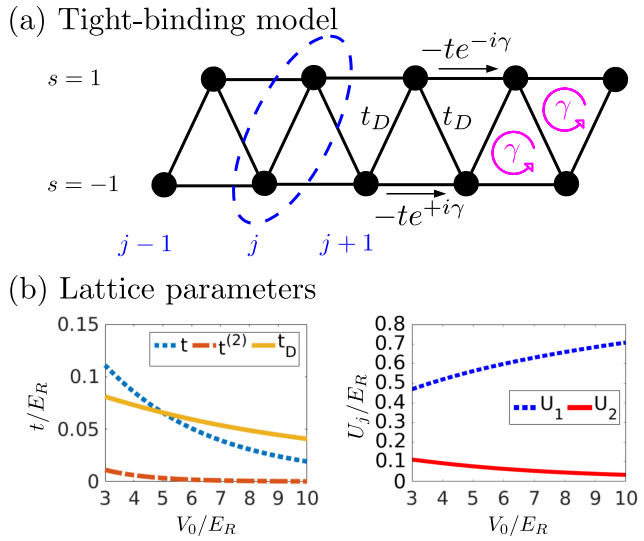

FIG. 1. (a) The semi-synthetic zigzag lattice corresponding to the tight-binding Hamiltonian (6). The lattice is affected by a non-staggered flux $\gamma = a\tilde{\kappa}/2 = \pi\tilde{\kappa}/\kappa$ over triangular plaquettes. (b) Tight-binding parameters. Left: Horizontal nearest neighbor (t) and next-nearest neighbor ($t^{(2)}$) hopping parameters together with diagonal tunneling strength t_D as a function of the scaled lattice depth V_0/E_R for $\Omega = 0.2020E_R$; Right: Normalized interactions U_1 and U_2 as a function of the scaled lattice depth.

ate the semi-synthetic zigzag lattice shown in Fig. 1(a), the atoms are confined in a one-dimensional periodic trapping potential $V \propto \pm\cos(\kappa x)$, opposite for each internal state. In addition, the two quasi-spin states are coupled by laser-induced transitions characterized by a Rabi frequency Ω and a recoil wave vector $\tilde{\kappa}\mathbf{e}_x$ aligned along the lattice direction $\mathbf{e}_x$. The resulting single-particle Hamiltonian is

$$H = \frac{\hat{p}^2}{2m} + \frac{V_0}{2}\cos(\kappa x)\,\sigma_z + \hbar\Omega\left(\sigma_+ e^{i\tilde{\kappa}x} + \sigma_- e^{-i\tilde{\kappa}x}\right), \quad (1)$$

where V_0 is the height of the trapping potential while σ_z and $\sigma_\pm = \sigma_x \pm i\sigma_y$ denote the standard Pauli spin matrices and combinations thereof.

The out-of-phase optical lattice can be produced by taking the quasi-spin states with $s = \pm 1$ to be the ground state $^1S_0$ and the long-lived excited state $^3P_0$ of the alkaline-earth(-like) atoms, such as Ytterbium [15] or Strontium [40, 41], for which the excited state has a typical lifetime far exceeding the experimental time scale [7, 15, 40, 42]. In contrast to the recent experiments [15, 40], the atoms are to be trapped at an anti-magic (rather than magic) wavelength to have the opposite trapping potentials for the two atomic internal states. Alternatively, one may use two Raman-coupled hyperfine atomic states $|F, m_F\rangle$ with projections $m_F = 0$ and $m_F = -1$ from the $F = 1$ ground-state manifold of the ^{87}Rb atoms [43] as the two quasi-spin states (see Fig. 2). The lattice potential $V \propto \pm\cos(\kappa z)$ is then obtained by

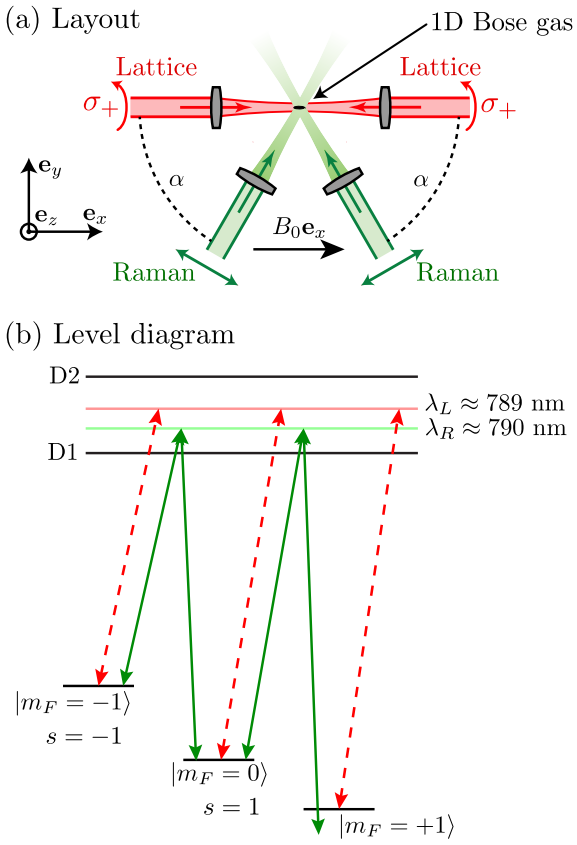

FIG. 2. (a) Schematic layout of proposed experimental setup. A bias magnetic field $\mathbf{B}_0 = B_0\mathbf{e}_x$ Zeeman-splits the hyperfine spin states of ^{87}Rb atoms. A counter-propagating pair of σ_+ polarized laser beams (shown in red) with $\lambda_L = 4\pi/\kappa \approx 789$ nm form a spin-dependent lattice with opposite signs for atoms in the $m_F = -1$ and $m_F = 0$ states [8, 38, 39]. This traps the $|F = 1, m_F = -1, 0\rangle$ states on lattice sites shifted by half the lattice constant $a/2 = \pi/\kappa$ providing a semi-synthetic zigzag lattice. Two horizontally polarized lasers (shown in red) at $\lambda_R = 2\pi/\tilde{\kappa} \approx 790$ nm resonantly couple the two spin states producing the flux $\gamma = \tilde{\kappa}a/2 = \pi/2$ tuned by taking the angle $\alpha \approx 60°$ between the laser beams. (b) Level diagram. The σ_+ polarized lattice laser beams (dashed red arrows) shift individual m_F states, but do not drive transitions. The strength of the state-dependent contribution to this shift is maximized when the beams propagate parallel to $\mathbf{B}_0$. The Raman lasers (solid green arrows) are tuned to be in resonance with $m_F = -1 \to 0$ transition, but detuned from the $m_F = 0 \to +1$ transition. Note that the Zeeman splitting of the ground state $F = 1$ hyperfine manifold is shown on a greatly exaggerated scale.

balancing the vector and scalar light shifts of a state-dependent lattice [8, 38]. This can be done by using a standing wave of a circularly (either σ_+ or σ_-) polarized light, and detuning slightly away from the frequency at which the scalar light shift is exactly zero.

B. Tight binding approximation

We focus on a sufficiently deep lattice potential with the depth V_0 typically exceeding the recoil energy $E_R = \hbar^2\kappa^2/8m$ five times. In this regime, a tight-binding approach is appropriate. We use the index j to label the sites along the physical (long) direction, and the internal states with $s = \pm 1$ are interpreted as sites along the synthetic dimension [11]. This provides a semi-synthetic zigzag lattice depicted in Fig. 1(a).

To proceed with the tight-binding approach, we introduce the Wannier functions $w_j(x)$ for the atomic motion in the one-dimensional cosine potential $V(x) = V_0\cos(\kappa x)/2$ oscillating with the spatial periodicity $a = 2\pi/\kappa$. The functions $w_j(x) \equiv w_0(x - ja)$ are localized at the potential minima $x_j = aj$. The Wannier basis for the two spin states with $s = \pm 1$ is thus given by

$$w_{s,j}(x) = w_0(x - sa/4 - ja), \tag{2}$$

where for convenience the origin of the x axis has been shifted to the midpoint between the neighboring $s = \pm 1$ sites. The locations of the opposite spin states differ by $a/2$, i. e. by a half of the lattice constant.

Matrix elements for tunneling along the real dimension have the usual form

$$-t = \int w^*_{s,j+1}(x)\left[\frac{\hat{p}^2}{2m} - \frac{V_0}{2}\cos(\kappa x)\right] w_{s,j}(x)\,dx. \tag{3}$$

With the minus sign absorbed into the definition in Eq. (3), the quantity t is real and positive. Matrix elements for the laser-assisted tunneling along the two "diagonal" directions of the semi-synthetic lattice are obtained by overlapping the Wannier functions weighted with the position-dependent laser coupling term:

$$\int w^*_{1,j}(x)\,\Omega\,e^{i\tilde{\kappa}x} w_{-1,j}(x)\,dx = t_D\,e^{i\tilde{\kappa}aj}, \tag{4a}$$

and

$$\int w^*_{1,j+1}(x)\,\Omega\,e^{i\tilde{\kappa}x} w_{-1,j}(x)\,dx = t_D\,e^{i\tilde{\kappa}a(j+1/2)}. \tag{4b}$$

Here the amplitude t_D is determined by both the Rabi frequency Ω and the overlap integral ρ between the neighboring Wannier functions for the opposite spin states:

$$t_D = \Omega\rho, \quad \rho = \int w_0^*(x - a/4)\,e^{i\tilde{\kappa}x}\,w_0(x + a/4)\,dx. \tag{5}$$

Within the tight-binding approach, we introduce the Bose operators $c_{s,j}$ and $c^\dagger_{s,j}$ to describe the annihilation and creation of atoms on the sites (s, j) of the semi-synthetic zigzag lattice. By adding appropriate phase factors to these operators $c_{s,j} \to c_{s,j}\,e^{-ijsa\tilde{\kappa}/2}$, one arrives at the tight-binding Hamiltonian with complex-valued tunneling elements $e^{\pm isa\tilde{\kappa}/2}$ along the long direction (real dimension) and real-valued tunneling t_D along the diagonal semi-synthetic directions:

$$\begin{aligned} H = {} & t_D \sum_j \left[c^\dagger_{1,j}c_{-1,j} + c^\dagger_{1,j-1}c_{-1,j}\right] \\ & - t\sum_{j,s} c^\dagger_{s,j+1}c_{s,j}\,e^{-isa\tilde{\kappa}/2} + \text{H.c.}. \end{aligned} \tag{6}$$

Here the first contribution describes the diagonal (spin-flip) tunneling in the semi-synthetic lattice. The lattice is affected by a non-staggered flux $\gamma = a\tilde{\kappa}/2 = \pi\tilde{\kappa}/\kappa$ over triangular plaquettes due to the recoil, as illustrated in Fig. 1(a).

Figure 1(b) displays the dependence of the tunneling parameters t and t_D on the lattice depth for the characteristic value of the Rabi frequency $\Omega = 0.2020\,E_R$. This particular choice of the laser strength leads to equal values of the two hopping parameters $t = t_D$ for the lattice depth $V_0 = 5E_R$ subsequently used in the many-body calculations. Note that the ratio t_D/t is tunable and increases linearly with the Rabi frequency Ω. Couplings between more distant sites are much smaller and can be safely neglected.

C. Single particle spectrum

In terms of the momentum-space bosonic operators $\hat{c}^{(\dagger)}_{s,k}$ the Hamiltonian reads

$$H = \sum_k \begin{pmatrix}\hat{c}^\dagger_{1,k} & \hat{c}^\dagger_{-1,k}\end{pmatrix}\begin{pmatrix}h_{11} & h_{12}\\ h_{21} & h_{22}\end{pmatrix}\begin{pmatrix}\hat{c}_{1,k}\\ \hat{c}_{-1,k}\end{pmatrix}, \tag{7}$$

where $h_{12} = h_{21} = 2t_D\cos(ka/2)$ and $h_{jj} = -2t\cos[ka + \gamma(-1)^j]$, with the row index $j = 1, 2$. To develop more intuition into the single-particle properties of the model, let us look at the case where $\tilde{\kappa} = \kappa/2$. The flux over a triangular plaquette is then $\gamma = \pi/2$, so that the time-reversal symmetry is broken in the semi-synthetic lattice even though the flux over a full elementary cell evaluates to $2\gamma = \pi$. In passing we note that the time-reversal symmetry is preserved if the triangular plaquette of the zigzag lattice is pierced by a π flux [44]. Returning to the situation where $\gamma = \pi/2$, the two dispersion branches read

$$\epsilon_\pm(k) = \pm 2\sqrt{t^2\sin^2(ka) + t_D^2\cos^2(ka/2)}. \tag{8}$$

The tight-binding dispersion (8) is in a good agreement with the exact band structure shown in Fig. 3 for the zigzag lattice with $\tilde{\kappa} = \kappa/2$ and $V_0 = 5E_R$ corresponding to $\gamma = \pi/2$, $t = 0.0658E_R$ and $\rho = 0.3258$, with different values of Ω determining $t_D = \Omega\rho$. It is noteworthy that the dispersion becomes quartic around $k = 0$ for $t_D = t_{D,\text{critical}} = 2t$ which corresponds to the critical Rabi frequency $\Omega_{\text{critical}} = 2t/\rho$. For the lattice depth $V_0 = 5E_R$ the critical Rabi frequency is $\Omega_{\text{critical}} = 0.4039\,E_R$, and the resulting band structure is shown in Fig. 3(c). Below the critical value, $t_D < 2t$, there are two

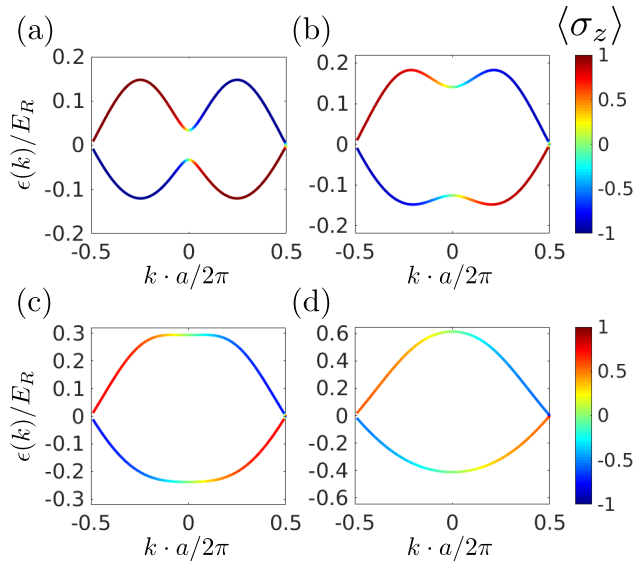

FIG. 3. Exactly calculated dispersion curves for $V_0 = 5\,E_R$, $\kappa = 2\tilde{\kappa}$ ($\gamma = \pi/2$) and various strengths of the spin-flip coupling: (a) $\Omega = 0.05$, (b) $\Omega = 0.2020$, (c) $\Omega = 0.4039E_R$ (the critical value), and (d) $\Omega = 0.8E_R$. This corresponds to: (a) $t_D = 0.25t$, (b) $t_D = t$, (c) $t_D = 2t$ (quartic dispersion at $k = 0$), and (d) $t_D = 4t$.

symmetric minima at $ka = \pm\arccos[(t_D/2t)^2]$. Above the critical value, $t_D > 2t$, there is a single minimum at $k = 0$.

We stress that the plots in Fig. 3 represent the exact calculations which agree well with the tight-binding model for Ω up to the critical value $\Omega_{\rm critical}$ and a little above it. Yet for $\Omega = 0.8E_R \approx 2\Omega_{\rm critical}$ (i.e. for $\Omega\rho \approx 4t$), there is already a marked deviation from the tight-binding model due to mixing with higher orbital bands. In fact, since the gap between the first and the second orbital bands is of the order of $2E_R$ at $V_0 = 5E_R$, the inter-band coupling becomes relevant only for larger Ω which is comparable to E_R, such as for $\Omega = 0.8E_R$. This is approximately the regime where Zhou and Cui [45] also saw deviations from the tight-binding model for a square semi-synthetic lattice.

The spin magnetization $\langle\sigma_z\rangle$ of the eigenstates is indicated by color in Fig. 3. The red and blue colors correspond to a fully magnetized state with $s = 1$ and $s = -1$, respectively. In the case of weak coupling (upper panels) the dispersion has a double-well shape with a clear spin separation in different minima. For stronger coupling the spin states get increasingly mixed. At the critical value $\Omega = 0.4039E_R$, the double well transforms to a single-minimum shape with a strong spin mixture.

D. Bloch oscillations

A characteristic feature of the zigzag lattice is the crossing of the two energy bands at the edges of the Brillouin zone $ka = \pm\pi$. In Fig. 3 we see that there is no band gap at these points and the spin polarization is preserved when moving from one energy band to the other at the Brillouin zone boundary $ka = \pm\pi$. This is also true for other values of the flux γ. The absence of the gap is a consequence of the invariance of the Hamiltonian (1) under the spatial translation by half the lattice period $a/2$ followed by time reversal, the latter representing a spin flip combined with an inversion of the Peierls phase $\gamma \to -\gamma$ [46]. As a result, the period of Bloch oscillations is doubled, cf. Ref. 47.

To illustrate the observable consequences of symmetry-related doubling of the Brillouin zone, we performed a numerical simulation of a wave packet in the zigzag lattice. We prepared a Gaussian wave packet composed entirely of the states from the lower energy band close to $k = 0$ and initially situated at a certain position (referred to as site $j = 0$) in the real space. Under the influence of a lattice tilt the wave packet is scanning the single-particle band structure while transferring diabatically between the two energy bands at the edges of the Brillouin zone. The results of our numerical simulation are shown in Fig. 4(a) for the specific choice $t_D = t$, and clearly indicate the doubling of the Bloch period. To further clarify this effect, we contrast these results to those shown in Fig. 4(b) in which the onsite energies are modified by an additional spin-dependent bias $0.3\,t\sigma_z$. In such a situation the single-particle bands acquire small gaps at the Brillouin zone boundaries. As a consequence, the wave packet is split with the atoms being partially transferred into the other band each time the Brillouin zone boundary is reached.

III. MANY-BODY EFFECTS

A. Interaction Hamiltonian

To take interactions into account, the tight binding Hamiltonian (7) is complemented with the interaction term

$$H_{\rm int} = \frac{U_1}{2}\sum_{j,s} n_{s,j}(n_{s,j}-1) + U_2\sum_j [n_{1,j}+n_{1,j-1}]\,n_{-1,j}, \tag{9}$$

where

$$U_1 = U_0\int |w_0(x)|^4\,dx \tag{10}$$

is the onsite interaction energy between atoms with the same spin states. On the other hand,

$$U_2 = U_0\int |w_0(x+a/4)|^2\,|w_0(x-a/4)|^2\,dx \tag{11}$$

represents the density-density interaction between atoms occupying neighboring sites with opposite spin states,

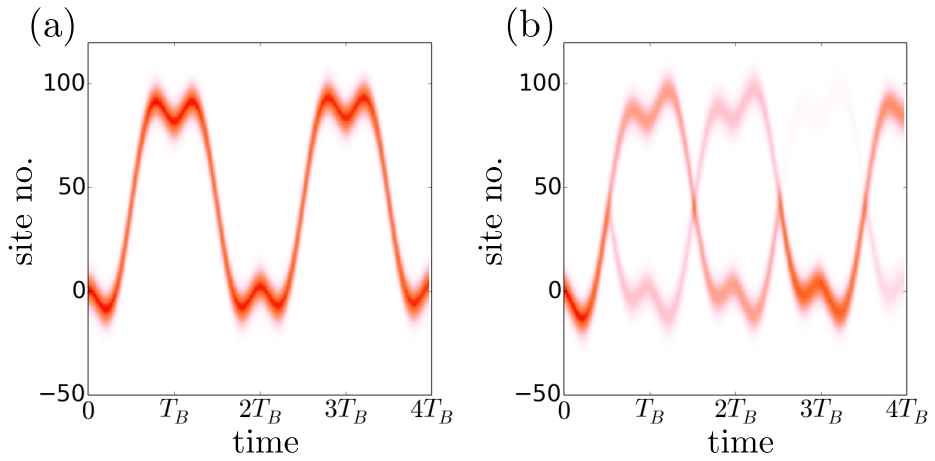

FIG. 4. Bloch oscillations for a Gaussian wave packet in a tilted zigzag lattice. Panel (a) corresponds to the band structure presented in Fig. 2(b) of the main text. In panel (b) the legs of the ladder legs are additionally biased by introducing a spin-dependent onsite energy shift $\pm 0.3\, t\sigma_z$, and the band gaps opened close to the Brillouin zone boundary lead to the Landau-Zener tunneling between the two bands.

i. e., the interactions acting along the diagonal links of the semi-synthetic zigzag lattice shown in Fig. 1(a). The prefactor U_0 is defined by the scattering length (assumed to be state-independent) and the confinement in the perpendicular (y, and z) spatial directions. The specific value of $U_0 \approx 1.09\, E_R$ used in our simulations was obtained for the perpendicular confinement depths of $30\, E_R$. In Fig. 1(b), we plot U_1 and U_2 as a function of the lattice depth showing that U_2 is around five times smaller than U_1 for a typical lattice height $V_0 = 5\, E_R$. On the other hand, interaction between the atoms at the neighboring sites with the same spin state is not included because it is much smaller than both U_1 and U_2.

B. Many-body phases

In our calculations we take the lattice height $V_0 = 5\, E_R$ for which the interaction energies read $U_1 \approx 0.56\, E_R$ and $U_2 \approx 0.074\, E_R$. To investigate the many-body phases supported by the semi-synthetic zigzag lattice we performed a series of numerical simulations based on the density-matrix renormalization group technique [36] using the open-source OSMPS code [48]. Our simulations targeted the ground states of lattices containing $L = 60$ sites (that is, 30 two-site unit cells) with open boundary conditions and fractional filling factors N/L corresponding to all integer particle numbers N up to 60. Working with such finite systems we were able to stay close to the experimentally feasible regime [49] while also maintaining a reasonable numerical effort. To check the scaling properties of the obtained results representative simulations were rerun also with larger lattice sizes containing up to 120 sites. The remaining two parameters whose values were tuned in a broad interval are the flux γ and the diagonal hopping parameter t_D. On the other hand, the values for the horizontal hopping parameter $t \approx 0.066\, E_R$ and the nearest-neighbor interaction strength U_2 were taken from the modeling of a lattice of depth $V_0 = 5E_R$ [cf. Fig. 1(b)]. Focusing on the effects brought about by the strong atom-atom interactions, in the main part of our calculations we chose to work in the limit of hardcore bosons. Thus, the onsite interaction strength $U_1 \approx 0.56\, E_R$ is regarded to be the dominant energy scale and is accounted for by restricting the number of bosons per lattice site to be not more than one. Having rerun the calculations with more than one boson per site we were able to confirm that the observed interesting many-body phases described below are indeed adequately represented by the hardcore limit.

The zigzag lattice offers a possibility to realize a tunable single-particle dispersion, seen in Fig. 3, by changing the ratio of the diagonal and horizontal tunneling parameters t_D/t. In the limits where one of these quantities significantly exceeds the other, $t_D \gg t$ or $t \gg t_D$, we observe quasicondensed phases signaled by the algebraic decay of the single-particle density matrix $g_1(i,j) \equiv \langle c_i^\dagger c_j \rangle$ as a function of the separation of sites $|i-j|$ [50]. In the limit of a dominant diagonal tunneling t_D, one obtains the usual quasicondensate at the single minimum at $k = 0$. Since the magnetic flux is not absorbed into the internal structure of the quasicondensate wave function with $k = 0$, the chiral currents are induced in the legs of the lattice [49, 51]. This phase supported by the zigzag lattice corresponds to the one observed in square ladders [49, 51]. It has been termed the *Meissner phase* in analogy to the physics of superconductors. In the opposite limit of weakly coupled spin-polarized legs – that is, when the horizontal hopping t is dominant – we find a striped phase analogous to the *vortex phase* formed in square ladders [49, 51]. Here, the current and density oscillations are induced by the interference of partial quasicon-

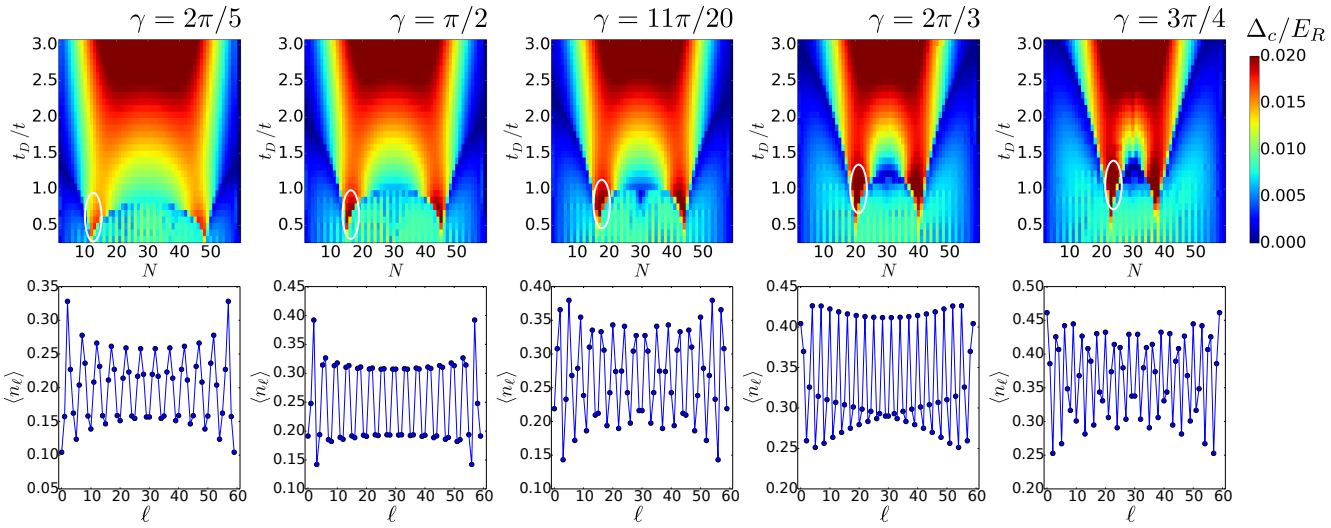

FIG. 5. Many-body phase diagram of the zigzag lattice for a set of flux values $\gamma = \{0.4\,\pi, 0.5\,\pi, 0.55\,\pi, \frac{2}{3}\pi, \frac{3}{4}\pi\}$. Top row: the scaled charge gap Δ_c/E_R plotted as a function of the number of particles N in the lattice of size $L = 60$ and the ratio of the hopping strengths t_D/t. Areas corresponding to enhanced charge gaps close to $t_D \approx t$ and the filling factor $N/L = \gamma/2\pi$ are conspicuous and are marked with white ovals. Bottom row: the expectation of the site occupation $\langle n_\ell \rangle$ versus the site number ℓ calculated at the phase-diagram points inside the white ovals.

densates occupying the two minima in the single-particle band structure. While this qualitative picture is strictly valid for non-interacting bosons it does survive also in the presence of finite interactions. Let us also stress that in the thermodynamic limit (as opposed to finite-size simulations) the gapless vortex phase is expected to support oscillations in the density correlations and not the density itself.

In between the two limits supporting quasicondensed ground states there lies an intriguing regime of balanced tunneling strengths $t \sim t_D$ associated with the presence of kinetic frustration. In particular, when $t = t_D$ each triangular plaquette is characterized by the absence of a weak link that could absorb the complex phase accumulated while encircling the plaquette. Under such circumstances the role of the atom-atom interactions will be enhanced, which might drive the system into a gapped phase. Indeed, our simulations show that the power-law decay of the single-particle density matrix $g_1(i,j)$ is replaced by an exponential decay signaling the destruction of the quasicondensed phase. To complement these observations, in Fig. 5 we plot the behavior of the charge gap [52] $\Delta_c(N) = E_{N+1} + E_{N-1} - 2E_N$ calculated from the ground-state energies of the zigzag lattice with a varying number of particles. In the top row, the coordinate axes represent the two governing parameters, the filling factor N/L (with $L = 60$) plotted on the horizontal axis and the ratio of the hopping parameters t_D/t plotted on the vertical axis. The series of five phase diagrams represent a subset of calculations performed on a dense set of different values of the flux γ.

The phase diagrams reveal the emergence of areas – marked with white ovals – where charge gaps are significantly enhanced. It is noteworthy that these gapped "islands" are situated precisely at the parameter values where the single-particle correlations decay exponentially and the filling factor assumes flux-dependent values $N/L = \gamma/2\pi$ and $N/L = 1 - \gamma/2\pi$. These two values are related by the particle-hole symmetry brought about by the hardcore constraint. They correspond precisely to the situation with one particle or hole per magnetic unit cell containing $2\pi/\gamma$ triangular lattice plaquettes or $2\pi/\gamma$ sites, like in the integer bosonic Hall effect [53–56].

The bottom row of panels in Fig. 5 shows the particle density oscillations calculated at points taken from inside the white ovals. Here, the expectation value of the density $\langle n_\ell \rangle$ is plotted as a function of the site index $0 \leqslant \ell \leqslant 59$. We see that for any value of the scaled flux γ and the corresponding flux-dependent filling $N/L = \gamma/2\pi$, the density oscillations occur at the wavelength corresponding to one particle per oscillation. For example, in the second column we look at $\gamma = \pi/2$ and the filling $N/L = 1/4$, thus implying $N = 15$ for $L = 60$. Here we count 15 full oscillations of the density, each covering four sites. Note that the observed density wave is fundamentally different from a gapped phase with staggered density modulation, which is directly favored by strong nearest-neighbor interactions U_2 and found at half filling (see the following subsection), since it occurs on longer wavelengths dictated by the magnetic flux. Nevertheless, a finite value of U_2 enhances the charge gap of the flux-induced density wave. As seen in the plots corresponding to $\gamma = 2\pi/5$ and $\gamma = 2\pi/3$, periodicities of three and five sites are also possible. The remaining two panels are calculated at $\gamma = 11\pi/20$ and $\gamma = 3\pi/4$. Here, according to the general observed trend

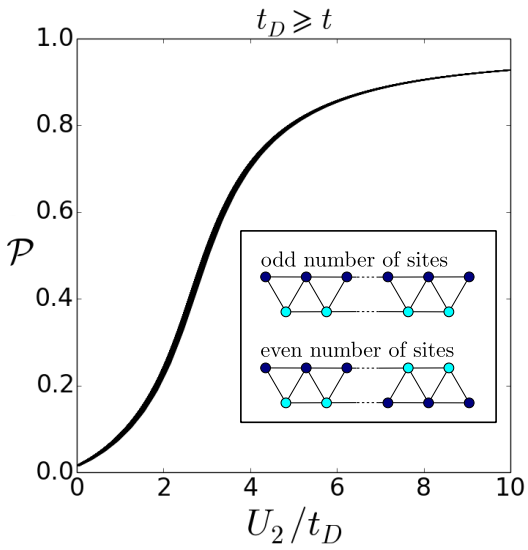

FIG. 6. The spin polarization $\mathcal{P}$ as a function of the nearest-neighbor repulsion strength calculated for $N = 30$ particles on a zigzag lattice of $L = 59$ sites without the artificial flux. When diagonal transitions dominate over the horizontal transitions, $t_D \geqslant t$ the shown dependence of the polarization $\mathcal{P}$ becomes insensitive to the relative magnitude of t. The thick line is a superposition of many dependencies with the ratio of the hopping parameters $1 \leqslant t_D/t \leqslant 20$.

one expects an incommensurate filling of, respectively, 16.5 and 22.5 particles per 60 sites. Although the density distributions look less regular in these cases, one still observes the formation of a density wave following the same predictive pattern. The required filling corresponds to the density where the magnetic unit length matches the wavelength of Friedel oscillations [57] in a system of free fermions, to which the simulated system can be mapped for $t = U_2 = 0$. Friedel oscillations occur near local defects, such as the boundary of the system, and decay algebraically. One can see in Fig. 5 that (at finite U_2) they are promoted to a long-ranged density wave and persist across the sample, when a commensurate magnetic length is introduced with a finite value of t.

C. Spin polarization

As a further example of the many-body physics supported by the zigzag lattice we look at the spin polarization induced by the strong nearest-neighbor interactions. Here, we work at the average filling N/L close to one half and in the absence of the artificial flux, $\gamma = 0$. In the presence of nearest-neighbor interaction — which is a distinguishing feature of the zigzag configuration — the particles are expected to occupy every second site thereby preferentially flocking onto one of the ladder legs and inducing non-zero net spin polarization defined as $\mathcal{P} = (n_\uparrow - n_\downarrow)/(n_\uparrow + n_\downarrow)$. A numerical calculation reveals that in this particular case the supported ground state configuration is sensitive to the total number of sites being even or odd. The effect can be explained in a simple way as the tendency of strong interactions to push particles into the sharp corners formed at the ends of the finite lattice. This is illustrated in the inset of Fig. 6 where the dark (light) blue color is used to mark preferentially occupied (depleted) lattice sites. Obviously, if the total number of sites L is even, the boundary conditions lead to opposite preferred spin polarizations at the two ends of the finite lattice, and the polarization must change sign somewhere in the middle of the lattice. In contrast, when the total number of sites is odd, the boundary conditions facilitate the largely uniform spin polarization of the whole lattice.

As a matter of fact, whether or not such a spin-polarized configuration will be formed depends on the competition of the nearest-neighbor repulsion and the delocalizing effect of inter-site hopping. The results of our numerical simulations performed on the system of $N = 30$ hardcore particles on a lattice of $L = 59$ sites are presented in Fig. 6. It is striking that as soon as $t_D \geqslant t$ the behavior of the spin polarization $\mathcal{P}$ shows a universal behavior – it depends only on the the ratio U_2/t_D and is virtually independent of the strength of the relatively weaker spin-preserving transitions with the parameter $t \leqslant t_D$. The thick line shown in Fig. 6 is in fact a superposition of many dependencies with the ratio of the hopping parameters $1 \leqslant t_D/t \leqslant 20$. In the complementary regime $t \geqslant t_D$, spin-preserving hopping transitions start to contribute to the melting of the spin-polarized state. Here, relatively stronger interactions are needed to induce the spin imbalance, and the polarization $\mathcal{P}$ depends on both U_2/t and U_2/t_D and thus loses its universal behavior.

IV. SUMMARY

We proposed a scheme for the realization of a semi-synthetic zigzag optical lattice built from a one-dimensional spin-dependent optical lattice with transitions between internal atomic states. Each of the lattice's triangular plaquettes ensnares the same—tunable—magnetic flux that can controllably deform the single-particle band structure form the single-minimum to the double-well configuration. In the proposed setup, the atom-atom interactions are nonlocal in both dimensions and stabilize density-wave-like phases at flux-dependent filling factors.

We thank Immanuel Bloch, Alessio Celi, Xiaoling Cui, Simon Fölling, Sebastian Greschner, Maciej Lewenstein, Michael Lohse, Pietro Massignan, Leonardo Mazza, Shuyan Wu, and Jakub Zakrzewski for helpful discussions. This research was supported by the Lithuanian Research Council (Grant No. MIP-086/2015) and by the German Research Foundation (DFG) via the Research

Unit FOR 2414. I. B. S. was partially supported by the ARO's Atomtronics MURI, by AFOSR's Quantum Matter MURI, NIST, and the NSF through the PCF at the JQI. C. S. is grateful for support by the Studienstiftung des deutschen Volkes.

[1] M. Lewenstein, A. Sanpera, V. Ahufinger, B. Damski, A. Sen (De), and U. Sen, "Ultracold atomic gases in optical lattices: Mimicking condensed matter physics and beyond," Adv. Phys. **56**, 243–379 (2007).

[2] I. Bloch, J. Dalibard, and W. Zwerger, "Many-body physics with ultracold gases," Rev. Mod. Phys. **80**, 885–964 (2008).

[3] M. Lewenstein, A. Sanpera, and V. Ahufinger, *Ultracold atoms in optical lattices: Simulating quantum many-body systems* (Oxford University Press, 2012).

[4] J. Javanainen and J. Ruostekoski, "Optical detection of fractional particle number in an atomic Fermi-Dirac gas," Phys. Rev. Lett. **91**, 150404 (2003).

[5] D. Jaksch and P. Zoller, "Creation of effective magnetic fields in optical lattices: the Hofstadter butterfly for cold neutral atoms," New J. Phys. **5**, 56 (2003).

[6] K. Osterloh, M. Baig, L. Santos, P. Zoller, and M. Lewenstein, "Cold atoms in non-Abelian gauge potentials: From the Hofstadter "moth" to lattice gauge theory," Phys. Rev. Lett. **95**, 010403 (2005).

[7] J. Dalibard, F. Gerbier, G. Juzeliūnas, and P. Öhberg, "Colloquium: Artificial gauge potentials for neutral atoms," Rev. Mod. Phys. **83**, 1523–1543 (2011).

[8] N. Goldman, G. Juzeliūnas, P. Öhberg, and I. B. Spielman, "Light-induced gauge fields for ultracold atoms," Rep. Prog. Phys. **77**, 126401 (2014).

[9] N. Goldman, J. C. Budich, and P. Zoller, "Topological quantum matter with ultracold gases in optical lattices," Nat. Phys. **12**, 639–645 (2016).

[10] O. Boada, A. Celi, J. I. Latorre, and M. Lewenstein, "Quantum simulation of an extra dimension," Phys. Rev. Lett. **108**, 133001 (2012).

[11] A. Celi, P. Massignan, J. Ruseckas, N. Goldman, I. B. Spielman, G. Juzeliūnas, and M. Lewenstein, "Synthetic gauge fields in synthetic dimensions," Phys. Rev. Lett. **112**, 043001 (2014).

[12] H. M. Price, O. Zilberberg, T. Ozawa, I. Carusotto, and N. Goldman, "Four-dimensional quantum Hall effect with ultracold atoms," Phys. Rev. Lett. **115**, 195303 (2015).

[13] M. Mancini, G. Pagano, G. Cappellini, L. Livi, M. Rider, J. Catani, C. Sias, P. Zoller, M. Inguscio, M. Dalmonte, and L. Fallani, "Observation of chiral edge states with neutral fermions in synthetic Hall ribbons," Science **349**, 1510–1513 (2015).

[14] B. K. Stuhl, H.-I. Lu, L. M. Aycock, D. Genkina, and I. B. Spielman, "Visualizing edge states with an atomic Bose gas in the quantum Hall regime," Science **349**, 1514–1518 (2015).

[15] L. F. Livi, G. Cappellini, M. Diem, L. Franchi, C. Clivati, M. Frittelli, F. Levi, D. Calonico, J. Catani, M. Inguscio, and L. Fallani, "Synthetic dimensions and spin-orbit coupling with an optical clock transition," (2016), arXiv:1609.04800 [cond-mat.quant-gas].

[16] F. A. An, E. J. Meier, and B. Gadway, "Direct observation of chiral currents and magnetic reflection in atomic flux lattices," (2016), arXiv:1609.09467 [cond-mat.quant-gas].

[17] T.-S. Zeng, C. Wang, and H. Zhai, "Charge pumping of interacting fermion atoms in the synthetic dimension," Phys. Rev. Lett. **115**, 095302 (2015).

[18] S. K. Ghosh, U. K. Yadav, and V. B. Shenoy, "Baryon squishing in synthetic dimensions by effective SU(M) gauge fields," Phys. Rev. A **92**, 051602(R) (2015).

[19] N. R. Cooper and A. M. Rey, "Adiabatic control of atomic dressed states for transport and sensing," Phys. Rev. A **92**, 021401(R) (2015).

[20] On a single-particle level, a possibility of creating a non-square semi-synthetic geometry was recently considered by D. Suszalski and J. Zakrzewski, "Different lattice geometries with synthetic dimension," Phys. Rev. A **94**, 033602 (2016). The proposal relies on experimentally more challenging additional diagonal tunnelings between the original sites of a semi-synthetic square lattice.

[21] R. W. Chhajlany, P. R. Grzybowski, J. Stasińska, M. Lewenstein, and O. Dutta, "Hidden string order in a hole superconductor with extended correlated hopping," Phys. Rev. Lett. **116**, 225303 (2016).

[22] T. Graß, C. Muschik, A. Celi, R. W. Chhajlany, and M. Lewenstein, "Synthetic magnetic fluxes and topological order in one-dimensional spin systems," Phys. Rev. A **91**, 063612 (2015).

[23] D. Greif, G. Jotzu, M. Messer, R. Desbuquois, and T. Esslinger, "Formation and dynamics of antiferromagnetic correlations in tunable optical lattices," Phys. Rev. Lett. **115**, 260401 (2015).

[24] R. G. Hulet, P. M. Duarte, R. A. Hart, and T.-L. Yang, "Antiferromagnetism with ultracold atoms," (2015), arXiv:1512.05311 [cond-mat.quant-gas].

[25] M. Boll, T. A. Hilker, G. Salomon, A. Omran, I. Bloch, and C. Gross, "Spin and charge resolved quantum gas microscopy of antiferromagnetic order in Hubbard chains," (2016), arXiv:1605.05661 [cond-mat.quant-gas].

[26] L. W. Cheuk, M. A. Nichols, K. R. Lawrence, M. Okan, H. Zhang, E. Khatami, N. Trivedi, T. Paiva, M. Rigol, and M. W. Zwierlein, "Observation of spatial charge and spin correlations in the 2D Fermi-Hubbard model," (2016), arXiv:1606.04089 [cond-mat.quant-gas].

[27] T. Lahaye, C. Menotti, L. Santos, M. Lewenstein, and T. Pfau, "The physics of dipolar bosonic quantum gases," Rep. Prog. Phys. **72**, 126401 (2009).

[28] B. Yan, S. A. Moses, B. Gadway, J. P. Covey, K. R. A. Hazzard, A. Maria Rey, D. S. Jin, and J. Ye, "Observation of dipolar spin-exchange interactions with lattice-confined polar molecules," Nature **501**, 521–525 (2013).

[29] A. Frisch, M. Mark, K. Aikawa, S. Baier, R. Grimm, A. Petrov, S. Kotochigova, G. Quéméner, M. Lepers, O. Dulieu, and F. Ferlaino, "Ultracold dipolar molecules composed of strongly magnetic atoms," Phys. Rev. Lett. **115**, 203201 (2015).

[30] S. Baier, M. J. Mark, D. Petter, K. Aikawa, L. Chomaz, Z. Cai, M. Baranov, P. Zoller, and F. Ferlaino, "Ex-

tended Bose-Hubbard models with ultracold magnetic atoms," Science **352**, 201–205 (2016).
[31] G. Pupillo, A. Micheli, M. Boninsegni, I. Lesanovsky, and P. Zoller, "Strongly correlated gases of Rydberg-dressed atoms: Quantum and classical dynamics," Phys. Rev. Lett. **104**, 223002 (2010).
[32] M. Viteau, M. G. Bason, J. Radogostowicz, N. Malossi, D. Ciampini, O. Morsch, and E. Arimondo, "Rydberg excitations in Bose-Einstein condensates in quasi-one-dimensional potentials and optical lattices," Phys. Rev. Lett. **107**, 060402 (2011).
[33] A. W. Glaetzle, M. Dalmonte, R. Nath, C. Gross, I. Bloch, and P. Zoller, "Designing frustrated quantum magnets with laser-dressed Rydberg atoms," Phys. Rev. Lett. **114**, 173002 (2015).
[34] H. Labuhn, D. Barredo, S. Ravets, S. de Léséleuc, T. Macrì, T. Lahaye, and A. Browaeys, "Tunable two-dimensional arrays of single Rydberg atoms for realizing quantum Ising models," Nature **534**, 667–670 (2016).
[35] G. Vidal, "Efficient simulation of one-dimensional quantum many-body systems," Phys. Rev. Lett. **93**, 040502 (2004).
[36] U. Schollwöck, "The density-matrix renormalization group in the age of matrix product states," Ann. Phys. **326**, 96–192 (2011).
[37] R. Orús, "A practical introduction to tensor networks: Matrix product states and projected entangled pair states," Ann. Phys. **349**, 117–158 (2014).
[38] I. H. Deutsch and P. S. Jessen, "Quantum-state control in optical lattices," Phys. Rev. A **57**, 1972–1986 (1998).
[39] D. McKay and B. DeMarco, "Thermometry with spin-dependent lattices," New J. Phys. **12**, 055013 (2010).
[40] S. Kolkowitz, S. L. Bromley, T. Bothwell, M. L. Wall, G. E. Marti, A. P. Koller, X. Zhang, A. M. Rey, and J. Ye, "Spin-orbit coupled fermions in an optical lattice clock," (2016), arXiv:1608.03854 [cond-mat.quant-gas].
[41] M. L. Wall, A. P. Koller, S. Li, X. Zhang, N. R. Cooper, J. Ye, and A. M. Rey, "Synthetic spin-orbit coupling in an optical lattice clock," Phys. Rev. Lett. **116**, 035301 (2016).
[42] F. Gerbier and J. Dalibard, "Gauge fields for ultracold atoms in optical superlattices," New J. Phys. **12**, 033007 (2010).
[43] Y-J. Lin, K. Jiménez-García, and I. B. Spielman, "Spin-orbit-coupled Bose-Einstein condensates," Nature **471**, 83–86 (2011).
[44] S. Greschner, L. Santos, and T. Vekua, "Ultracold bosons in zig-zag optical lattices," Phys. Rev. A **87**, 033609 (2013).
[45] L. Zhou and X. Cui, "Spin-orbit coupled ultracold gases in optical lattices: High-band physics and insufficiency of tight-binding models," Phys. Rev. B **92**, 140502(R) (2015).
[46] In this discussion we are employing a usual definition of the time reversal symmetry involving the complex conjugation and spin reversal. On the other hand, in the tight binding picture the spin states are treated as sites in an extra dimension making a semi-synthetic zigzag lattice. Adopting such a point of view the time-reversal symmetry no longer involves the spin flip and thus has another meaning. This kind of the 'time-reversal symmetry' is implied in the paragraph following Eq. (7).
[47] R. Khomeriki and S. Flach, "Landau-Zener Bloch oscillations with perturbed flat bands," Phys. Rev. Lett. **116**, 245301 (2016).
[48] M. L. Wall and L. D. Carr, "Out-of-equilibrium dynamics with matrix product states," New J. Phys. **14**, 125015 (2012).
[49] M. Atala, M. Aidelsburger, M. Lohse, J. T. Barreiro, B. Paredes, and I. Bloch, "Observation of chiral currents with ultracold atoms in bosonic ladders," Nat. Phys. **10**, 588–593 (2014).
[50] In performing calculations we represent the zigzag lattice as a one-dimensional array of sites enumerated consecutively along a zigzag-shaped path.
[51] M. Piraud, F. Heidrich-Meisner, I. P. McCulloch, S. Greschner, T. Vekua, and U. Schollwöck, "Vortex and Meissner phases of strongly-interacting bosons on a two-leg ladder," Phys. Rev. B **91**, 140406(R) (2015).
[52] D. Rossini and R. Fazio, "Phase diagram of the extended Bose-Hubbard model," New J. Phys. **14**, 065012 (2012).
[53] T. Senthil and M. Levin, "Integer quantum Hall effect for bosons," Phys. Rev. Lett. **110**, 046801 (2013).
[54] S. Furukawa and M. Ueda, "Integer quantum Hall state in two-component Bose gases in a synthetic magnetic field," Phys. Rev. Lett. **111**, 090401 (2013).
[55] Y.-H. Wu and J. K. Jain, "Quantum Hall effect of two-component bosons at fractional and integral fillings," Phys. Rev. B **87**, 245123 (2013).
[56] Y.-C. He, S. Bhattacharjee, R. Moessner, and F. Pollmann, "Bosonic integer quantum Hall effect in an interacting lattice model," Phys. Rev. Lett. **115**, 116803 (2015).
[57] J. Friedel, "Metallic alloys," Nuovo Cimento **7**, 287–311 (1958).